Talanta 81 (2010) 1670–1675

Contents lists available at ScienceDirect

Talanta

journal homepage: www.elsevier.com/locate/talanta

A vapor sensor array using multiple localized surface plasmon resonance bands in a single UV–vis spectrum

Kuan-Jen Chen, Chia-Jung Lu*

Department of Chemistry, National Taiwan Normal University, Taipei 11677, Taiwan, ROC

ARTICLE INFO

Article history:
Received 4 February 2010
Received in revised form 9 March 2010
Accepted 10 March 2010
Available online 19 March 2010

Keywords:
Localized surface plasmon resonance
VOCs
Sensor array
Nanoparticles

ABSTRACT

This research reports a sensor array consisting of three types of surface-modified nanoparticles that exhibit localized surface plasmon resonance (LSPR) extinctions at different wavelength regions of a UV–vis spectrum. By simultaneously measuring the ensemble of the LSPR bands of the three nanomaterials, response patterns were obtained at different regions of a UV–vis spectrum. Three types of nanometals used in this study were Ag nanoparticles, Au nanoparticles and Au nano-shells. The center wavelengths of their LSPR bands were 427, 534 and 772 nm respectively, after they were each modified with decanethiol, naphthalene thiol and 2-mercaptobenzothiazole to create chemical selectivity. The average absolute difference in the absorbance of each LSPR band was used as the signal for each sensor. Reversible, rapid (~8 s) and wide linear range responses were observed with this sensor array. Nine volatile organic compounds (VOCs) with various functional groups were tested with this sensor array and differentiable groups of response patterns were obtained. The detection limits were as low as 16 ppm for anisole.

1. Introduction

The explosive development of nano-materials in recent decades has opened new windows for chemical sensor research. The performance of many well-known types of sensor material has been dramatically improved by the adoption of a nano-structure. This improvement is due mostly to a larger surface area or to better structural stability [1]. Also, novel chemical sensors have been developed based on the properties of newly synthesized nanomaterials. For example, monolayer-protected metal nanoparticles have been successfully applied as chemiresistors and in quartz crystal microbalance for VOC detection [2–7].

Localized surface plasmon resonance (LSPR) is another interesting property of metal nanoparticles. It is a collective charge oscillation that can be induced by electromagnetic radiation in the UV–vis wavelength range. The LSPR of metal nanoparticles can be readily measured through UV–vis spectrometry as an absorbance (or extinction) band [8,9]. Both the peak wavelength and the absorbance of the LSPR band are sensitive to the environmental refractive index surrounding the nanoparticles [10–12]. Extensive research has been devoted to developing sensors using LSPR for the biomedical detection of proteins, sugars and disease diagnostics [13–20]. There are also non-biomedical applications of LSPR sensors such as detecting aqueous ammonia [21] and pH measurements [22]. The integration of a LSPR sensor into a microfluidic chip has also been reported recently [23].

In gas phase detection, Pacey and co-workers have demonstrated the detection of ozone using the LSPR of gold nanoislands [24]. Rubinstein and co-workers reported polystyrene-coated nano-gold islands on a glass substrate for organic vapor sensing [25]. Our earlier studies focused on an initial sensing mechanism for unmodified nanoparticles and on tuning selectivity by a surface thiolate self-assembled monolayer (SAM) on silver nanoparticles [26,27].

By far, the chemical or biological selectivity of LSPR sensors was mostly created via surface modification on same type of nanoparticle. Since the LSPR band of a given metal nanoparticle occupies a certain wavelength region in a UV–vis spectrum, it was difficult to "simultaneously" collect array responses of different surface-modified nanoparticles unless multiple spectrometers or costly optical switching mechanisms were used. Therefore, in the present study we proposed and tested an approach to collect multiple LSPR signals as an array in a single UV–vis spectrum using ensembles of different nano-metals. The selectivity for different VOCs can be expressed in different wavelength regions of a UV–vis spectrum. Cluster analysis was used to classify the vapor response patterns generated by the LSPR sensor array.

2. Experimental

2.1. Nanoparticle synthesis

Gold nanoparticles were prepared through the reduction of hydrogen tetrachlororaurate ($HAuCl_4$, Alfa Aesar) in an aqueous phase. A 100 mL aqueous solution of 1 mM $HAuCl_4$ was boiled with

* Corresponding author. Tel.: +886 2 77346132; fax: +886 2 29324249.
E-mail address: cjlu@ntnu.edu.tw (C.-J. Lu).

0039-9140/$ – see front matter © 2010 Elsevier B.V. All rights reserved.
doi:10.1016/j.talanta.2010.03.023

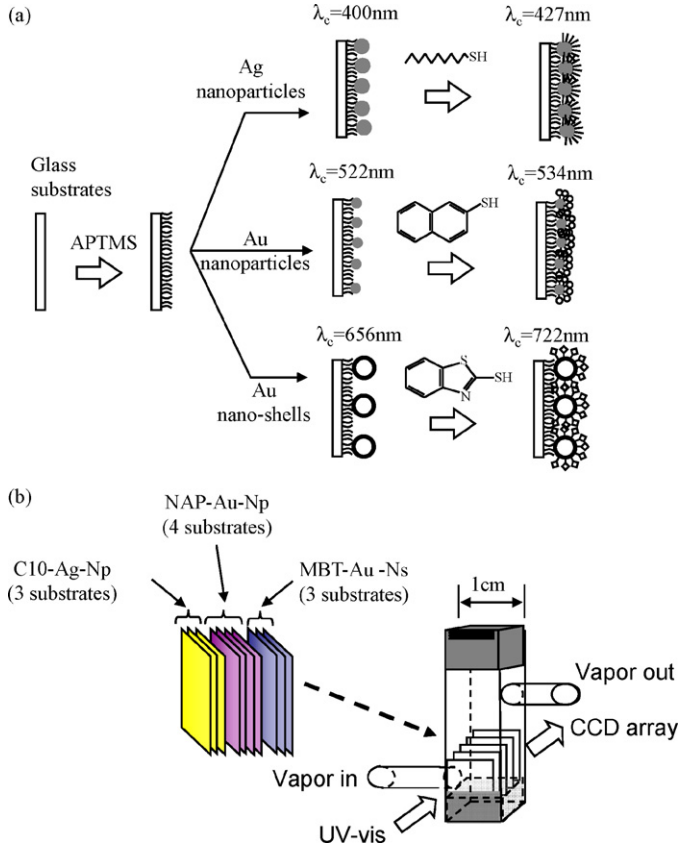

Fig. 1. Scheme of building LSPR sensor array: (a) sensor substrate fabrications and (b) array assembly in a flow-cell cube.

vigorous stirring in a round-bottom flask, to which 10 mL of 40 mM citric sodium was added. The solution was continuously boiled for 10 min, and the color of the solution slowly turned from yellow to purple-red. The solution was cooled at room temperature and stored in a refrigerator at 4 °C for further use.

Silver nanoparticles were synthesized by the reduction of $AgNO_3$ in an ethylene glycol solution containing polyvinylpyrolidone (PVP). In 10 mL ethylene glycol, 2 g of PVP were dissolved, and then 130 mg of $AgNO_3$ were added and stirred until completely dissolved. The solution was slowly heated and refluxed at 120 °C until the color turned to dark yellow. The solution was then cooled and stored in a refrigerator.

Gold nano-shells were synthesized using silver nanoparticles as a template [28]. The surface atoms of silver nanoparticles were gradually replaced by gold through the addition of $HAuCl_4$ aqueous solution. Deionized water (20 mL) was used to dilute 1 mL of silver nanoparticle solution. A solution of $HAuCl_4$ (3.2 mM) was slowly dripped into a boiling silver nanoparticle solution until the color turned blue. The solution was then cooled at room temperature. White AgCl precipitate was removed by centrifuge.

2.2. Assembly of nanoparticle monolayers on glass substrates

The process for the following experiments is illustrated in Fig. 1a. Cover glass substrates were cleaned with a Piranha solution, rinsed with deionized water, and then dried in an oven at 100 °C for 10 min. The glass substrates were immersed in a 10% solution of 3-aminopropyl-trimethoxysilane (APTMS) in ethanol for 1 h and then were rinsed thoroughly with ethanol and deionized water to remove unreacted APTMS [29,30]. Glass substrates were then immersed in a solution containing metal nanoparticles and kept in a refrigerator for 24 h. The image of the nanoparticle-immobilized layer on glass was measured by Field Emission Scanning Electron Microscope (FESEM, JSM-6500F). The LSPR absorbance band was measured using a CCD array-type UV–vis spectrometer (USB2000, Ocean Optics).

2.3. Surface modification of metal nanoparticles

Three separated 0.1 M stock solutions of thiolate were prepared by dissolving decane thiol (C10), naphthalene thiol (NAP), and 2-mercaptobenzothiazole (MBT) in ethanol. The reaction solution for surface modification was prepared by diluting a 10 μL stock solution in 4 mL of ethanol. The final concentration of the reacting solution was 2.5×10^{-4} M of thiolates. The glass substrates with metal nanoparticle monolayers on the surface were immersed in reacting solution. After the thiolate had formed a self-assembled monolayer on the metal nanoparticle surface (~30 min), the substrates were rinsed thoroughly with ethanol until the center wavelength of the LSPR band had reached a steady value. The thiolate-modified sensor substrates were blown dry and preserved in nitrogen.

2.4. Sensor testing and vapor-generation system

Assembly of the LSPR array was achieved by placing a different number of the nanoparticle modified substrates in the holder. We custom-made a stainless-steel 10-slide holder that fits in an optical cube with gas-flow tubing coming in/out from the literal sides. Then, we inserted 3 slides of C10–Ag-nanoparticles, 4 slides of NAP–Au-nanoparticles, and 3 slides of MBT–Au-nano-shells into the holder and positioned them into the light path (Fig. 1b). A dynamic vapor-generation system was constructed with mass flow controllers, Teflon or stainless tubing, an organic solvent bubbler, and a mixing chamber. Test vapor concentrations were generated by adjusting the flow ratio between the saturated vapor flow and the clean air flow. The test flows into the UV–vis detection cell were switched between the clean air and the vapor concentration flow by computer controller solenoid valves. Details regarding the construction and calibration of the vapor generation system were described in our previous report [8,26].

3. Results and discussion

Fig. 2 shows the FESEM images of three nanoparticles after they formed an immobilized layer on glass substrates. The particle diameter of silver nanoparticles (Ag-Np) was 35 ± 9 nm (Fig. 2a). Gold nanoparticles (Au-Np) had a narrower size distribution, and the average particle size was also smaller (18 ± 4 nm, Fig. 2b). Au nano-shells (Au-Ns) were built from Ag nanoparticle templates. They were inherently larger in diameter (50 ± 12 nm, Fig. 2c) and widespread in particle size distribution. Both Ag-Np and Au-Ns occasionally showed some aggregation of a few nanoparticles. We suspect this can be attributed to the use of PVP. Although this polymer was designated as a protector for nanoparticles in solution, there was a chance that the long and polar chain of PVP might glue the particles together during the process of adsorption on glass—where nanoparticles and PVP are more concentrated than they were in solution. This local aggregation was also a source of LSPR band broadening. Nath and Chilkoti have investigated the LSPR sensitivity of Au nanoparticles with different diameters. It was found that sensitivity increased as the particle diameter increased from 13 to 39 nm and then reached a plateau for larger particles [19]. In the present study, we focused on one mean size for each type of nanoparticle.

The LSPR spectrums of the three nanoparticles after they were immobilized on glass that had been surface-modified with thiolates and exposed to 4000 ppm of m-xylene are separately shown

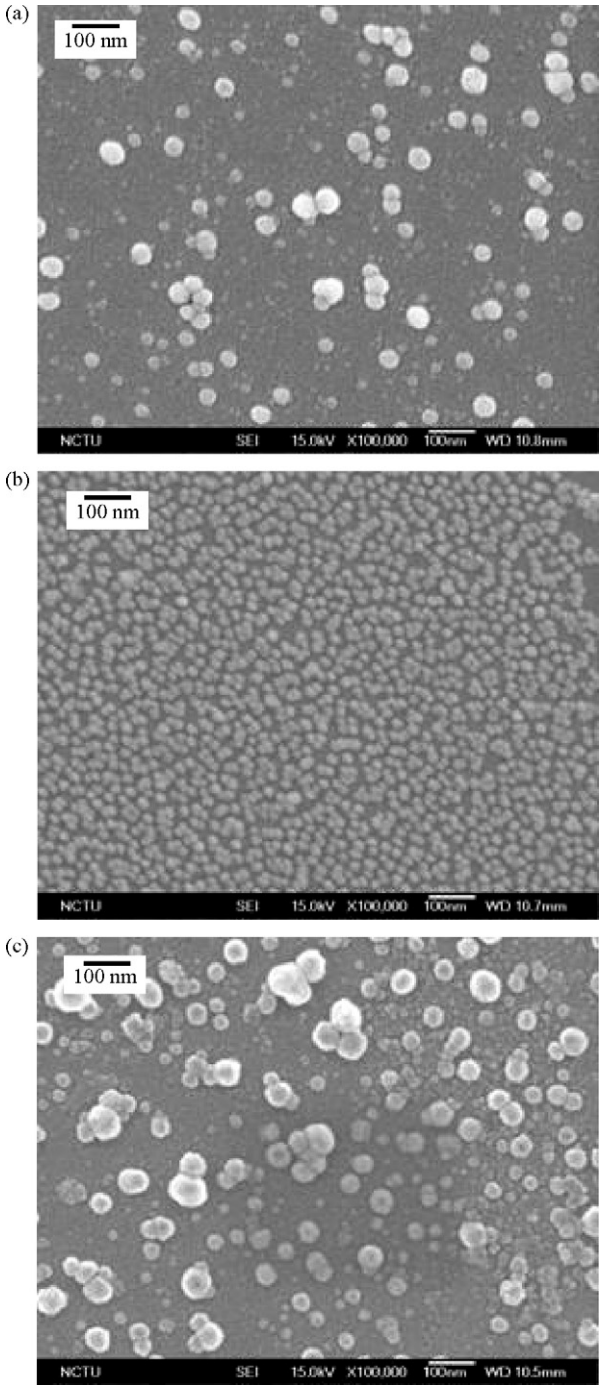

Fig. 2. FESEM images of nano-metal particles after being immobilized on glass substrates. (a) Ag nanoparticles, (b) Au nanoparticles, and (c) Au nano-shells.

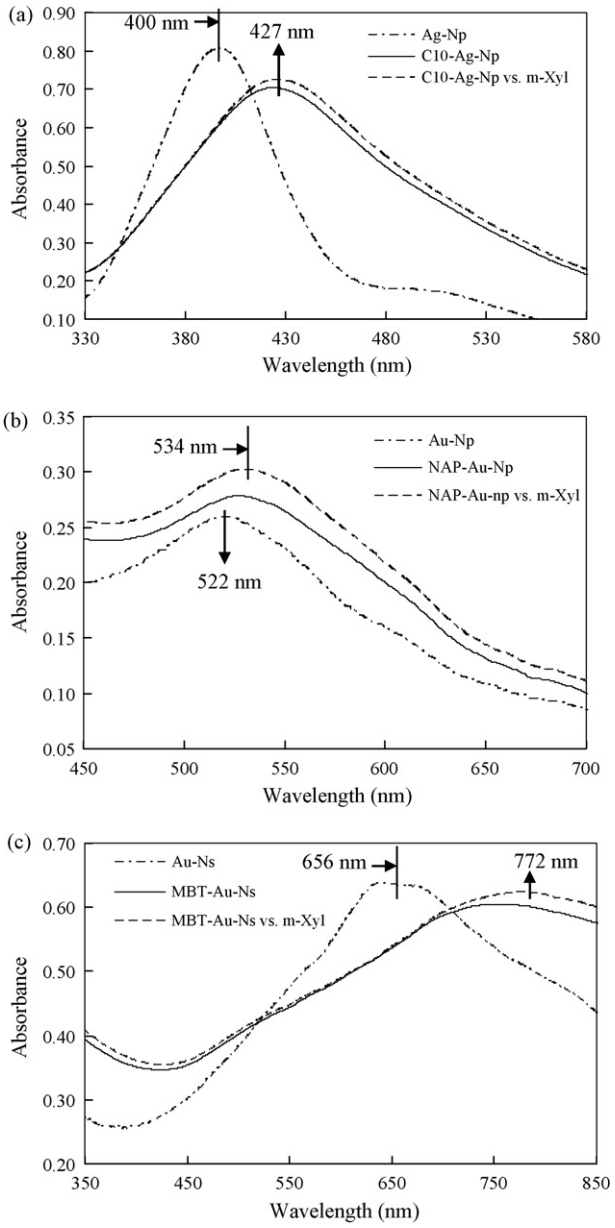

Fig. 3. Individual LSPR spectrums of (a) silver nanoparticles, (b) gold nanoparticles, or (c) gold nano-shells showing the stepwise changes after surface modification and exposure to 4000 ppm of m-xylene.

in Fig. 3. All three nanoparticles showed a significant red-shift and a band broadening after surface modification. The spectrums of LSPR after surface modification were taken after sensor substrates were thoroughly rinsed with ethanol and dried. This procedure was repeated until the center wavelength of LSPR reached a steady value. Thus, any unreacted thiols should have been removed leaving only those thiols that were chemically bonded to the metal surface. Gold nano-shells showed the greatest red-shift sensitivity to the surface modification (red-shift ~106 nm, Fig. 3c). Sun and Xia discussed this high sensitivity and explained that larger surface area and responses on both the inside and the outside of the shells are the reasons for this high sensitivity [28]. Compared with gold nano-shells, silver and gold nanoparticles have a relatively small red-shift following the surface modification (27 and 12 nm, Fig. 3a and b). Although the different refractive indexes of chemically adsorbed thiolates might have contributed to these differences in red-shift, our previous study has shown that the inherent sensitivity difference among these three nano-metals was the predominant factor. Their red-shift sensitivities toward the surface refractive indexes were 71.7 nm/RIU for Ag-Np, 32.7 nm/RIU for Au-Np, and 249.8 nm/RIU for Au-Ns [26]. When exposed to 4000 ppm of m-xylene, we observed a smaller increase of absorbance and red-shift in the LSPR spectrums for all three nanoparticles. The vapor response signals were expressed in both wavelength shifts and absorbance increases.

Fig. 4 shows the combined spectrum of the LSPR array employing three types of surface-modified nanoparticles. Due to the broadness of these individual LSPR bands, some overlaps were inevitable. However, the peaks of the three LSPR bands can still

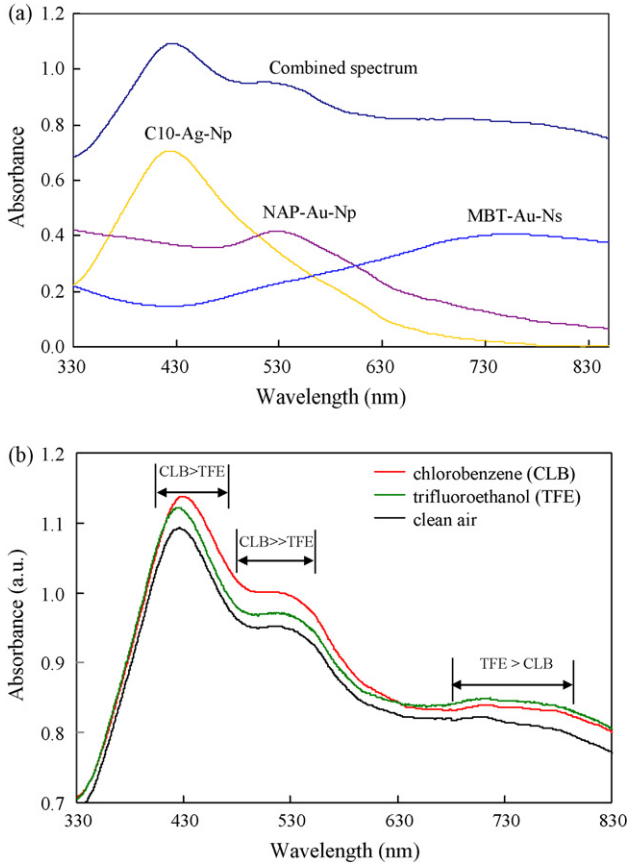

Fig. 4. (a) Individual spectrums of three LSPR sensors and the combined spectrum of the array. (b) Different sensitivities between chlorobenzene and 2,2,2-trifluoroethanol in three wavelength regions of each sensor.

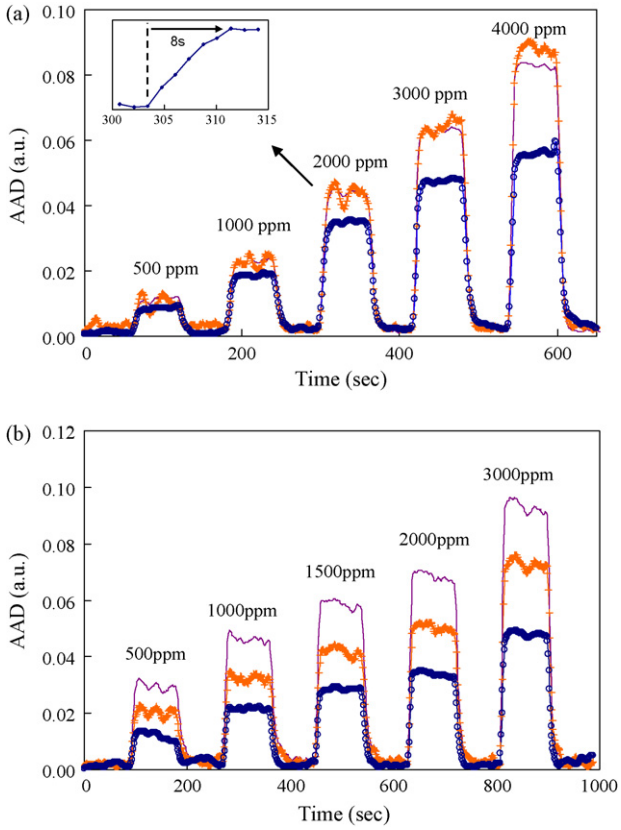

Fig. 5. Real-time response signals of three different wavelength regions of combined LSPR spectrum tested with (a) m-xylene, insert shows the magnified response curves of NAP–Au-Np at 2000 ppm and (b) n-pentanol (wavelength regions: +, 395–475 nm; –, 480–620 nm; ○, 690–850 nm).

be clearly identified in the combined spectrum. The peaks at 427, 534 and 772 nm represent different types of nano-metals with different surface modifications. Therefore, when the array was exposed to VOCs, different sensitivities should be seen at different wavelength regions. High concentrations of chlorobenzene (9000 ppm) and 2,2,2-trifluoroethanol (25 000 ppm) were used here to enhance the visibility of responses in this UV–vis spectrum. Under these test conditions, the 395–475 nm region showed a response to chlorobenzene that was only slightly higher than to 2,2,2-trifluoroethanol. The 480–620 nm region, however, showed a much higher absorbance increase for chlororbenzene, while the 690–850 nm region was more sensitive to 2,2,2-trifluoroethanol.

In order to take advantage of the entire absorbance band as the source of the signal, we used the averaged absorbance differences (AAD) rather than single-point absorbance changes as the sensor signal. The equation for calculating the AAD is as follows:

$$\mathrm{AAD} = \frac{\sum_{\lambda=\lambda_1}^{\lambda_n} A_\lambda - A_\lambda^0}{n}$$

where λ_1 and λ_n represent the left and right wavelength limits of a selected LSPR sensing region. A_λ is the absorbance at wavelength λ with vapor exposure and A_λ^0 is the absorbance in clean air at the same wavelength. n is the total number of data points in the selected region. As a result, the AAD averages the spectrum noise across the selected region in the same units as the absorbance. One advantage of using the AAD over peak shift or peak absorbance increase is that the precise peak wavelength of the LSPR band need not be determined. This is especially convenient when the vapor response signal includes both absorbance and small peak wavelength changes (Fig. 3). A limitation of using AAD as response signal is that it can only be used when the wavelength change is small. If a dramatic wavelength shift occurs, such as those changes due to surface modification, the AAD signal might not be linear versus the changes of the chemical environment surrounding nanoparticles.

Fig. 5 shows the real-time AAD response signals when the LSPR arrays were tested using various concentrations of m-xylene and 1-pentanol inside a dynamic vapor generation system. The left and right limits of each LSPR band are shown in the legend. The selection of the LSPR bandwidth (i.e., the number of data points) would not significantly change the relative signal height between sensors because the AAD is an averaged value. However, if the selected region is overly wide, a region with less response or a region overlapping another sensor might undermine the selectivity. For example, our selection of a wavelength region for a C10–Ag-Np response was 395–475 nm, and for a NAP–Au-Np response it was 480–620 nm. In fact, if a response above 480 nm was included into the C10–Ag-Np signal, we would incorporate a part of the NAP–Au-Np signal into C10–Ag-Np. The insert of Fig. 5a shows that it took approximately 8 s to reach 100% response. Rapid and reversible responses were observed with all test vapors and sensors, which indicates only physical adsorption was involved during the VOC–LSPR sensing process.

Nine VOCs with various functional groups were chosen to test the selectivity of this array. We included two less polar compounds (i.e., m-xylene and toluene), two chlorinated organics, and other compounds with different degrees of polarity. The calibration curves and reproducibility adaptations are presented in Table 1. The slopes of calibration show each sensor's relative selectivity to the test vapors. The R^2 values listed in this table also indicate this sensor array has good linearity for all tested vapors. Relative standard deviations (RSD) were determined for five replicates at each con-

Table 1
Equations of calibration curves and relative standard deviations of replicate measurements.

Vapors	C10–Ag-Np			NAP–Au-Np			MBT–Au-Ns		
	Calibration eqn.[a]	R^2	RSD[b]	Calibration eqn.	R^2	RSD	Calibration eqn.	R^2	RSD
1-Pentanol	$y = 2.02 \times 10^{-5} x + 8.94 \times 10^{-3}$	0.994	0.025	$y = 2.49 \times 10^{-5} x + 1.66 \times 10^{-2}$	0.997	0.012	$y = 1.44 \times 10^{-5} x + 3.79 \times 10^{-3}$	0.994	0.017
Anisole	$y = 2.76 \times 10^{-5} x + 1.88 \times 10^{-3}$	0.999	0.023	$y = 2.73 \times 10^{-5} x + 7.81 \times 10^{-4}$	0.998	0.014	$y = 2.16 \times 10^{-5} x + 1.74 \times 10^{-3}$	0.968	0.019
m-Xylene	$y = 2.22 \times 10^{-5} x - 3.52 \times 10^{-3}$	0.999	0.066	$y = 1.98 \times 10^{-5} x + 1.35 \times 10^{-3}$	0.999	0.025	$y = 1.33 \times 10^{-5} x + 3.55 \times 10^{-3}$	0.989	0.027
Chlorobenzene	$y = 1.24 \times 10^{-5} x + 1.78 \times 10^{-3}$	0.997	0.049	$y = 1.07 \times 10^{-5} x + 4.33 \times 10^{-3}$	0.994	0.016	$y = 6.71 \times 10^{-6} x + 3.36 \times 10^{-3}$	0.990	0.024
Pyridine	$y = 7.04 \times 10^{-6} x + 1.31 \times 10^{-2}$	0.996	0.034	$y = 9.62 \times 10^{-6} x + 2.36 \times 10^{-2}$	0.998	0.026	$y = 4.36 \times 10^{-6} x + 6.36 \times 10^{-3}$	0.999	0.034
Toluene	$y = 4.44 \times 10^{-6} x - 2.11 \times 10^{-4}$	0.999	0.029	$y = 3.82 \times 10^{-6} x + 2.39 \times 10^{-3}$	0.996	0.014	$y = 3.21 \times 10^{-6} x - 1.19 \times 10^{-3}$	0.982	0.018
1,4-Dioxane	$y = 1.95 \times 10^{-6} x - 3.89 \times 10^{-3}$	0.990	0.032	$y = 2.64 \times 10^{-6} x - 3.89 \times 10^{-4}$	0.999	0.022	$y = 1.26 \times 10^{-6} x - 2.67 \times 10^{-3}$	0.998	0.019
2,2,2-Trifluoroethanol	$y = 1.51 \times 10^{-6} x + 1.79 \times 10^{-2}$	0.991	0.027	$y = 5.00 \times 10^{-7} x + 5.20 \times 10^{-3}$	0.988	0.033	$y = 3.45 \times 10^{-6} x + 1.17 \times 10^{-3}$	0.996	0.024
Trichloroethylene	$y = 2.14 \times 10^{-6} x + 2.19 \times 10^{-3}$	0.995	0.028	$y = 2.76 \times 10^{-6} x + 9.68 \times 10^{-3}$	0.996	0.020	$y = 1.02 \times 10^{-6} x + 8.56 \times 10^{-3}$	0.988	0.020

[a] Test concentration (x) unit is ppm. The unit of AAD signal (y) is absorbance.
[b] RSD: averaged relative standard deviations were determined by five replicate measurements at each of five different concentration level.

Fig. 6. Cluster analysis for response patterns of nine tested VOCs using a LSPR sensor array.

centration level, which was then averaged across the calibration range. The variation for all sensors and test vapors were within a few percent. The C10–Ag-Np sensor looked less stable than the others. This was because the UV–vis light intensity was diminished in this shorter wavelength range due to the use of glass substrates.

We applied cluster analysis to classify these response data using SPSS 12.0 software (Fig. 6). It was clear that compounds could be broken down into three major groups. Of these groups, 2,2,2-trifluoroethanol could easily be distinguished while the benzo-group compounds, toluene, m-xylene, chlorobenzene, and anisole, were closer in distance. The rest of the higher polar compounds formed a separate group. Although there were only three sensors in this array, the cluster analysis showed that this LSPR array could still provide initial vapor classifications correlated to their chemical structure.

The test concentration range, vapor pressure, refractive index and detection limits of tested organic vapors are summarized in Table 2. It was clear that less volatile compounds had lower detection limits. The lowest detection limits (3σ) calculated here were 15–16 ppm for anisole and 1-pentanol when tested with an NAP–Au-Np sensor. These limits remained to be relatively high by comparison with commercially available gas sensors, such as the SnO_2 sensor, which is capable of detecting single-digit ppm VOCs. The detection limits of the LSPR array in the present study were 1–2 orders higher for moderate volatile compounds compared with that of commercial sensors. There are several possible solutions to improve the detection limits of LSPR–VOC sensors in the future, such as increasing the number of sensor substrates, employing fiber optics, or with the help of a preconcentrator. There are micro-preconcentrators that can generate a concentration pulse with >5000 amplification factors [31,32]. This can certainly make our LSPR sensor array applicable to field VOC detection in an industrial environment. In fact, prototype instruments that use a preconcentrator to improve sensor detection of other types have been reported in the literature [33,34].

The sensitivity of a surface-modified LSPR–VOC sensor was influenced by at least three factors: the first was the amount of VOC adsorbed on the nanoparticle surface. This was mainly determined by the volatility of the tested vapor and by the affinities between the functional groups of the surface thiolate and the VOCs. The low volatile compounds absorbed and condensed more easily on the surface; hence, they were more sensitive. The affinity between the functional groups determined their selectivity if the volatility was in the same range. One exception that can be seen in Table 2 is trichloroethylene. We believe that its heavier molecular weight (M.W. = 131) might condense easier compared with 2,2,2-trifluoroethanol (M.W. = 100) or 1,4-dioxane (M.W. = 88).

Table 2
Physical properties and detection limits of tested vapors.

Vapors	p_v (Torr)[a]	n_D^{20}	Test conc. (ppm)	LOD (ppm)		
				Ag-Np	Au-Np	Au-Ns
1-Pentanol	2.2	1.405	500–3000	38	16	95
Anisole	3.5	1.516	1000–3000	15	16	58
m-Xylene	8.3	1.497	500–4000	122	108	124
Chlorobenzene	12	1.524	1000–9000	247	139	156
Pyridine	20.7	1.509	1500–10 000	518	394	368
Toluene	28.5	1.497	4000–12 000	175	128	196
1,4-Dioxane	37	1.421	2600–16 000	1339	1144	2266
2,2,2-Trifluoroethanol	70	1.291	5000–25 000	1048	2487	185
Trichloroethylene	77	1.477	4700–25 000	424	222	323

[a] p_v: vapor pressure at 298 K; n_D^{20}: refractive index of condensed phase.

The second factor was the inherent LSPR sensitivity of a given type of nanoparticle toward its environmental refractive index. This might determine which sensor is always more sensitive than others. Fortunately, this can be adjusted by changing the substrate number of each type of nanoparticle in the array. The third factor was also the least important: the refractive index of VOC in its condensed phase (Table 1). Our previous study [26] had already demonstrated that this factor makes only a minor contribution to the signals after accounting for the first two factors described above.

4. Conclusions

The objective of this study was to demonstrate that the selective responses of a LSPR array using surface functionalized nanoparticles could be simultaneously measured in one UV–vis spectrum with careful arrangement of nanoparticles and surface modification. The results of the present study clearly show different sensitivities at discrete wavelength regions in a UV–vis spectrum when the array was tested with various VOCs. Alternative sensor designs for improving detection limits using optical fibers or a preconcentrator are underway.

Acknowledgements

The authors are indebted to Dr. Chi-Lin Li for his assistance on cluster analysis work. The funding for this project was provided by the National Science Council (NSC) of Taiwan, ROC under contract number NSC 98-2113-M-003-005-MY2.

References

[1] M.E. Franke, T.J. Koplin, U. Simon, Small 2 (2006) 36–50.
[2] H. Wohltjen, A.W. Snow, Anal. Chem. 70 (1998) 2856–2859.
[3] A.W. Snow, H. Wohltjen, Chem. Mater. 10 (1998) 947–949.
[4] W.H. Steinecker, M.P. Rowe, E.T. Zellers, Anal. Chem. 79 (2007) 4977–4986.
[5] Q.Y. Cai, E.T. Zellers, Anal. Chem. 74 (2002) 3533–3539.
[6] C.-Y. Yang, C.-L. Lin, C.-J. Lu, Anal. Chim. Acta 565 (2006) 17–26.
[7] C.-L. Li, C.-J. Lu, Talanta 79 (2009) 851–855.
[8] E. Hutter, J.H. Fendler, Adv. Mater. 16 (2004) 1685.
[9] Y.S. Shon, H.Y. Choi, M.S. Guerrero, C. Kwon, Plasmonics 4 (2009) 95–105.
[10] S. Underwood, P. Mulvaney, Langmuir 10 (1994) 3427–3430.
[11] K.L. Kelly, E. Coronado, L.L. Zhao, G.C. Schatz, J. Phys. Chem. B 107 (2003) 668–677.
[12] I. Doron-Mor, Z. Barkay, N. Filip-Granit, A. Vaskevich, I. Rubinstein, Chem. Mater. 16 (2004) 3476–3483.
[13] C.R. Yonzon, D.A. Stuart, X. Zhang, A.D. McFarland, C.L. Haynes, R.P. Van Duyne, Talanta 67 (2005) 438–448.
[14] K.A. Willets, R.P. Van Duyne, Annu. Rev. Phys. Chem. 58 (2007) 267–297.
[15] P.K. Jain, I.H. El-Sayed, M.A. El-Sayed, Nanotoday 2 (2007) 18–29.
[16] M. Scampicchio, C.A. Fuenmayor, S. Mannino, Talanta 79 (2009) 211–215.
[17] A.J. Haes, S. Zou, G.C. Schatz, R.P. Van Duyne, J. Phys. Chem. B 108 (2004) 109–116.
[18] P. Buecker, E. Trileva, M. Himmelhaus, R. Dahint, Langmuir 24 (2008) 8229–8239.
[19] N. Nath, A. Chilkoti, Anal. Chem. 76 (2004) 5370–5378.
[20] M. Vestergaard, K. Kerman, D.-K. Kim, H.M. Hiep, E. Tamiya, Talanta 74 (2008) 1038–1042.
[21] S.T. Dubas, V. Pimpan, Talanta 76 (2008) 29–33.
[22] M. Nuopponen, H. Tenhu, Langmuir 23 (2007) 5352–5357.
[23] C. Huang, K. Bonroy, G. Reekmans, W. Laureyn, K. Verhaegen, I. De Vlaminck, L. Lagae, G. Borghs, Biomed. Microdevices 11 (2009) 893–901.
[24] A.N. Pisarenko, W.U. Spendel, R.T. Taylor, J.D. Brown, J.A. Cox, G.E. Pacey, Talanta 80 (2009) 777–780.
[25] T. Karakouz, A. Vaskevich, I. Rubinstein, J. Phys. Chem. B 112 (2008) 14530–14538.
[26] C.-S. Cheng, Y.-Q. Chen, C.-J. Lu, Talanta 73 (2007) 358–365.
[27] Y.-Q. Chen, C.-J. Lu, Sens. Actuators B 135 (2009) 492–498.
[28] Y. Sun, Y. Xia, Anal. Chem. 74 (2002) 5297–5305.
[29] N. Nath, A. Chilkoti, Anal. Chem. 74 (2002) 504–509.
[30] T. Okamoto, I. Yamaguchi, T. Kobayashi, Opt. Lett. 25 (2000) 372–374.
[31] W.-T. Tain, S.W. Pan, C.-J. Lu, E.T. Zellers, J. Microelectromech. Syst. 12 (2003) 264–272.
[32] W.-T. Tain, H.K.L. Chan, S.W. Pan, C.-J. Lu, E.T. Zellers, J. Microelectromech. Syst. 14 (2005) 498–507.
[33] C.E. Davis, C.K. Ho, R.C. Hughes, M.L. Thomas, Sens. Actuators B 104 (2005) 207–216.
[34] W.A. Groves, E.d.T. Zellers, G.C. Frye, Anal. Chim. Acta 371 (1998) 131–143.